THE JOURNAL OF PHYSICAL CHEMISTRY A

A: Spectroscopy, Molecular Structure, and Quantum Chemistry

Does Tetrahydrofuran (THF) Behave like a Solvent or a Reactant in the Photolysis of Thionyl Chloride (ClSO) in Cyclohexane? A Transient Infrared Difference Study.

Meng-Chen Shih, and Li-Kang Chu

J. Phys. Chem. A, **Just Accepted Manuscript** • DOI: 10.1021/acs.jpca.8b03775 • Publication Date (Web): 29 May 2018

ACS Publications

is published by the American Chemical Society. 1155 Sixteenth Street N.W., Washington, DC 20036

Does Tetrahydrofuran (THF) Behave like a Solvent or a Reactant in the Photolysis of Thionyl Chloride (Cl_2SO) in Cyclohexane? A Transient Infrared Difference Study.

*Meng-Chen Shih and Li-Kang Chu**

Department of Chemistry, National Tsing Hua University, 101, Section 2, Kuang-Fu Road, Hsinchu, Taiwan 30013

Corresponding Author

* To whom correspondence should be addressed. Phone: 886-3-5715131 ext. 33396. Fax: 886-3-5711082. E-mail: lkchu@mx.nthu.edu.tw.

ABSTRACT

The photolysis of thionyl chloride (Cl_2SO) in pure cyclohexane (cHex) and in cHex with a small amount of tetrahydrofuran (THF) irradiated with 266 nm pulsed laser was investigated using time-resolved step-scan Fourier-transform spectroscopy. The density functional theory B3LYP, with the conductor-like polarizable continuum model to account for the effects of solvents, was employed to predict the molecular parameters of the relevant species. Monitoring the wavenumbers and infrared absorbances attributed to the [S,O] species and accounting for the stoichiometry revealed SO_2 to be the major oxygen-containing end product for the thermal decomposition of Cl_2SO. Upon successive irradiation with 266 nm pulsed laser, the major product, as detected by IR absorption, was S_2O with minor SO_3, which could be generated from the secondary reactions of the photolytic intermediate ClSO. The majority of the transient vibrational features upon 266 nm irradiation of the mixture of Cl_2SO/cHex was attributed to ClSO, characterized at 1155 cm^{-1}, coupled with a minor contribution of $(ClSO)_2$ at 1212 and 1173 cm^{-1}. For the mixture of Cl_2SO/THF/cHex, the transient population of ClSO was retained, but the amount of $(ClSO)_2$ was slightly reduced, coupled with a new upward feature at 1054 cm^{-1} that was plausibly attributed to the C–O–C asymmetric stretching mode of ClSO–THF complex. Upon the successive irradiation of the Cl_2SO/THF/cHex mixture, the amount of S_2O was also decreased. The observed complexes of THF with solutes suggested that THF should not be merely treated as a solvent but regarded as a coordination molecule in organic synthesis. The formation of the intermediate–THF complexes altered the reaction pathways, as well as the types and populations of the end products.

INTRODUCTION

The macroscopic properties of solvents, namely, their polarity, solubility, and proticity, are generally taken into consideration for organic syntheses in terms of the dispersing mediums. The choice of solvent provides specificity in solvent-selective organic synthesis[1,2,3] and solvent-dependent crystallization.[4] In addition, solvents can serve as coordination molecules to chelate the reactive reagents to form stable complexes and to trigger a given reaction, such as boron trifluoride tetrahydrofuran (BH_3-THF) complex for Yamaguchi–Hirao alkylation,[5] and aldehyde and ketone metal complexes in the catalysis.[6] In addition to the organic syntheses, the photolysis of metal carbonyl complexes has manifested the coordination capability of solvents to the photolytic intermediates using time-resolved infrared spectroscopy.[7,8,9,10] Both the molecules containing lone pair electrons or π electrons, such as benzene,[8] acetone,[8] and tetrahydrofuran (THF),[9] and the saturated nonpolar solvents, such as cyclohexane (cHex) and heptane,[7] are capable of serving as coordination moieties.

Thionyl chloride (Cl_2SO) is commonly used in organic synthesis, such as the conversion of carboxylic acids to acyl chlorides[11] and the transformation of sulfinic acids into sulfinyl chlorides.[12] In addition to the synthetic purposes, ultraviolet excitation ($\lambda < 300$ nm) of Cl_2SO leads to the electronic transitions of an overlap of $\sigma^*_{S-Cl} \leftarrow n_s$ and $\sigma^*_{S-O} \leftarrow n_s$ transitions peaking approximately at 244 nm ($\sigma = 7.1 \times 10^{-18}$ cm^2) and $\sigma^*_{S-Cl} \leftarrow n_{Cl}$ at 194 nm ($\sigma = 1.3 \times 10^{-17}$ cm^2),[13,14] respectively, followed by further photodissociation.[15,16] At 248 nm, the laser induced fluorescence and molecular beam experiments revealed that the two-body Cl-elimination (Eq. 1, >96.5 %) dominates with a minute contribution of molecular elimination (Eq. 2), yielding electronically-excited SO ($b^1\Sigma^+$),[15,16] in gas phase,

$$Cl_2SO \xrightarrow{248\ \mathrm{nm}} ClSO + Cl \qquad Cl-\mathrm{elimination} \qquad 96.5\% \qquad (1)$$

$$Cl_2 + SO(b^1\Sigma^+) \quad \text{Molecular elimination} \quad 3.5\ \% \qquad (2)$$

At 193 nm, an extra three-body dissociation generates two Cls and one SO, about 80% of the Cl_2SO depletion, with 17 % Cl-elimination and 3 % molecular elimination.[15,16] The photolytic intermediate ClSO in gaseous phase has been characterized at 1162.9 cm^{-1} using time-resolved infrared spectroscopy.[17]

THF has long been known as a coordination reagent to various transition metals.[18] A theoretical work proposed that the coordination of the solvent THF molecules to the Sm (II) center in the carbenoid was capable of catalyzing the cyclopropanation reactions.[19] However, the coordination ability of THF has rarely been taken into consideration in organic syntheses. In this work, the photolysis of Cl_2SO in cHex with and without the addition of THF at 266 nm was monitored with time-resolved step-scan Fourier-transform spectroscopy (TRSSFTS), which has been widely employed in recording the evolution of the vibrational features of atmospheric chemical reactions,[20,21] photochemistry of retinal proteins,[22,23] and photodissociation of the metal carbonyl complexes.[10,24] Coupled with the vibrational wavenumbers predicted by the density functional theory method (B3LYP), we assigned the transient photolytic intermediate ClSO at 1155 cm^{-1} and the cascading products $(ClSO)_2$ and ClSO–THF complex due to the self-reaction of ClSO and the reaction of ClSO with THF, respectively. The steady-state difference spectra upon successive 266-nm irradiation manifested an alteration in the end products in the presence of THF. We have therefore demonstrated that THF possesses the coordination ability and further changes the reaction pathways and their concomitant end products.

MATERIALS AND METHODS

Sample preparations.

For the steady-state measurements, the solution containing Cl_2SO in pure cHex was prepared by dissolving 20 μL Cl_2SO (≥98 %, Sigma-Aldrich) in 6 mL cHex (99 %, J. T. Baker) without pre-purification. The solution containing Cl_2SO/THF = 1/3 in cHex was prepared by dissolving 20 μL Cl_2SO and 60 μL THF (≥99 %, Echo) in 6 mL cyclohexane without pre-purification. For the time-resolved photolysis measurements, the solution containing Cl_2SO in pure cHex was prepared by dissolving 0.2 mL Cl_2SO in 60 mL cHex. The solution containing Cl_2SO/THF = 1/2 in cHex was prepared by dissolving 0.2 mL Cl_2SO and 0.4 mL THF in 60 mL cHex. The compositions of THF were not further enlarged to avoid absorption saturation, which would hamper the differentiation in the spectroscopic evolution.

Pulsed 266 nm excitation system.

A frequency-quadrupled Nd:YAG laser (LS-2137U, LOTIS Tii) operated at a repetition rate of 10 Hz served as a pulsed 266-nm excitation source. The laser flux was controlled at 2.67–3.14 mJ cm^{-2} for steady-state successive irradiation and 5.3 mJ cm^{-2} for transient absorption experiments before entering the CaF_2 window of the flow cell. The laser beam was overlapped with the probing infrared beam in the sample compartment of the Fourier-transform infrared spectrometer (Vertex 80, Bruker), as shown in **Figure 1**. A photodiode (DET10A/M, Thorlabs, 1 ns rise time) was employed to collect the laser scattering to serve as the trigger for acquiring the time-resolved difference infrared spectra.

Steady-state infrared absorption spectra.

Steady-state infrared absorption spectra were collected to differentiate the end products with and without 266-nm photolysis of Cl_2SO in different solvent mixtures for a given duration. The liquid samples were sandwiched in two CaF_2 windows (1-inch diameter, 2-mm thickness) separated by a Teflon spacer of 0.1-mm thickness and mounted in the detection compartment of

the spectrometer, as shown in **Figure 1**. The spectra were acquired with a Fourier-transform infrared spectrometer (Vertex 80, Bruker) operated in continuous-scan mode with a spectral resolution of 1 cm^{-1} upon averaging 16 scans for each spectrum.

Sample injection system for time-resolved experiments.

The sample solution was loaded in a 50-mL glass syringe driven by a stepwise linear motor (Legato100, KD Scientific). The syringe was connected to the right side of the flow cell (Demountable Liquid Cell, 162-1100, Pike) through Teflon tubes of 4-mm outer diameter. The optical length, defined by the thickness of the Teflon spacer in the flow cell, was 0.1 mm. The photolyzed waste flew out of the left side of the flow cell. The injection speed of the sample was set at 18 $\mu L\ s^{-1}$.

Time-resolved difference infrared spectra monitored with a step-scan Fourier-transform interferometer.

The time-resolved infrared difference spectra of Cl_2SO upon 266 nm photolysis were recorded with a Fourier-transform infrared spectrometer (Vertex 80, Bruker) operated in the step-scan mode. The data were acquired using the ac/dc coupling method.[20,22] In the absence of laser exposure, the dc-coupled signal from the mercury cadmium telluride (MCT) detector (3.5 ns, KMPV8-0.5-J1/DC, Kolmar Technologies) was sent to a voltage amplifier (SR560, Stanford Research System), coupled by dc; then the output signal from the SR560 was recorded by an external analog-to-digital convertor (20 MHz, 14 bits, Bruker) for the calculation of the background spectrum ($S_0(\bar{\nu})$) and for phase correction. In the presence of laser excitation, the dc-coupled signal from the MCT detector was sent to a voltage amplifier (SR560, Stanford Research System), coupled by ac, and further amplified by a factor of 10 with an electronic filter in the bandwidth of 300k Hz – 300 Hz. The output signal from SR560 at a given optical retardation δ, $\Delta I_t(\delta)$, was recorded by an external

analog-to-digital convertor (20 MHz, 14 bits, Bruker). Once the data acquisition was completed for all the optical retardations, the time-evolved single channel spectra, $\Delta S_t(\bar{\nu})$, were calculated via reverse Fourier transformation of the interferograms $\Delta I_t(\delta)$ at different time slots. The time-resolved difference infrared spectra were calculated using Eq. 3.

$$\Delta A_t(\bar{\nu}) = -\log\left[\frac{S_0(\bar{\nu}) + \Delta S_t(\bar{\nu})/10}{S_0(\bar{\nu})}\right] \quad (3)$$

The upward and downward features thus represent the production and depletion, respectively. To reduce the period of data acquisition and the use of solvents, we performed the undersampling by narrowing the spectral range with two optical filters (1550–990 cm^{-1} with LP-6900 nm from Spectrogon and A565 from CFDL) positioned in the midst of the infrared beam, and the corresponding undersampling factor was 10. The acquisition of the interferogram required 377 steps of the moving mirrors at a spectral resolution of 4 cm^{-1}. The experimental period of a single experiment was within 11 minutes for an average of 15 laser shots at a 10-Hz repetition rate. Identical experiments were performed twice and thrice for Cl_2SO/cHex and Cl_2SO/THF/cHex samples, respectively, to achieve better ratios of signal to noise.

THEORETICAL CALCULATIONS

The Gaussian 09 program[25] was employed to predict the absolute energies, equilibrium geometries, harmonic wavenumbers, and infrared absorption intensities of the relevant species in cHex with B3LYP, which employs Becke's three-parameter hybrid exchange functional with a correlation functional.[26,27] Dunning's correlation-consistent polarized valence triple-zeta basis sets, augmented with s, p, d, and f functions (aug-cc-pVTZ),[28,29] were applied in all calculations. To account for the effect of the solvents, the aforementioned calculations were performed using the conductor-like polarizable continuum model (C-PCM).[30]

The relevant species are listed in **Scheme 1**, and the absolute energies and vibrational wavenumbers of the S=O associated modes for [S,O] compounds and the C–O–C asymmetric stretching mode of the THF moiety for THF-containing complexes in cHex are summarized in **Table 1**. The geometries of these molecules are provided in the **Supporting Information**. The observed vibrational wavenumbers of the S=O stretching modes of the stable [S,O] species, including SO_2, S_2O, SO_3, and Cl_2SO, in cHex in this work were about 1% smaller than those observed in the gaseous phase.[31,32,33] The weak perturbation of cHex was reasonable, for cHex is a non-polar solvent and contains no lone electron pairs, which might coordinate to the solutes. Moreover, this observation was supported by studies on the dielectric constant dependent vibrational wavenumber changes for the NH stretching vibration of pyrrole[34] and hydrogen fluoride.[35] The vibrational wavenumbers decreased with increases in the dielectric constants (ε) of the solvents.[34,35] Since the dielectric constant of cHex was *ca.* 2,[36] a minute spectral shift toward the lower wavenumber of a given vibrational mode was expected. Moreover, the predicted vibrational wavenumbers of the aforementioned [S,O] molecules in cHex were consistent with those observed in cHex, with an average deviation less than 1%. As a result, the predicted wavenumbers were not manually scaled for comparison with the observed values for the spectral assignments in the following sections.

RESULTS AND DISCUSSIONS

Steady-state IR difference spectra of Cl_2SO in different solvent compositions upon successive irradiation at 266 nm.

The steady-state spectra of neat Cl_2SO, cyclohexane, and mixture of THF and cHex at 1400–1000 cm^{-1} are shown in **Figure 2**. The absorption of Cl_2SO at 1239 cm^{-1} was attributed to the S=O stretching mode. An intense band at 1345 and a weak band at 1146 cm^{-1} were attributed

to the asymmetric and symmetric S=O stretching modes of SO_2, which was gradually produced after the thermal decomposition of Cl_2SO. The bands of cHex at 1257 and 1039/1014 cm^{-1} were attributed to the CH_2 twisting and CH_2 rocking modes, respectively.[31] An extra band of the mixture of cHex and THF at 1075 cm^{-1} was attributed to the C–O–C asymmetric stretching mode of THF.[37]

Following the evolution of the difference spectra of Cl_2SO in cHex with time in the absence of the 266 nm laser (**Figure 3a**), we found a gradual depletion of Cl_2SO at 1239 cm^{-1}, coupled with the generation of SO_2, featured at 1345 cm^{-1} (strong) and 1146 cm^{-1} (very weak). This combination of depletion and generation plausibly resulted from the slow thermal decomposition of Cl_2SO, which led to the end products SO_2, SCl_2, and Cl_2,

$$2Cl_2SO \rightarrow SO_2 + Cl_2 + SCl_2 \qquad \Delta H = 97 \text{ kJ mol}^{-1} \qquad (4)$$

The heat of reaction (Eq. 4) was derived from our predicted absolute energies listed in **Table 1**, in which the solvent effect of cHex has been taken into consideration. Cl_2 is not infrared active, and the vibrational wavenumbers of SCl_2 were beyond the detection region. Accounting for the predicted infrared intensities of SO_2 (287 km mol^{-1}) and Cl_2SO (232 km mol^{-1}), which were similar within acceptable uncertainties, the absorbance decrease of Cl_2SO (*ca.* −0.050) and the absorbance increase of SO_2 (*ca.* +0.022) roughly obeyed the stoichiometry of Eq. 4; i.e., $-\Delta Cl_2SO : \Delta SO_2 = 2 : 1$.

When a small amount of THF was added to the Cl_2SO/cHex mixture without exposure to 266 nm laser, the evolution of the IR difference spectra was distinct, as shown in **Figure 3b**. New features at 1075 cm^{-1} (downward) and 1053 cm^{-1} (upward) appeared, in addition to the generation of SO_2, which was also observed in the Cl_2SO/cHex system (**Figure 3a**). Comparing the steady-state spectra of the mixture of cHex and THF in **Figure 2**, the depletion at 1075 cm^{-1} coincided with the C–O–C asymmetric stretching mode of THF. This result implied that the products of the

thermal decomposition of Cl_2SO could interact with THF and cause the depletion of the neat THF in cHex. Presumably, the upward bathochromic band at 1053 cm^{-1} would be attributed to the C–O–C stretching mode of the coordination complexes containing THF. Comparing the predicted wavenumbers in **Table 1**, the wavenumber of the C–O–C stretching mode of SCl_2–THF was 11.4-cm^{-1} bathochromic with respect to that of THF, supporting the consumption at 1075 cm^{-1} (downward) and generation at 1053 cm^{-1} (upward).

When the mixture of Cl_2SO/cHex was successively irradiated with 266 nm laser, the generation of SO_2 at 1345 cm^{-1} was suppressed and replaced with new intense features at 1381 and 1156 cm^{-1} (**Figure 3c**). Comparing the predicted and gaseous vibrational wavenumbers of the species containing [S,O], the observed bands at 1381 cm^{-1} and 1156 cm^{-1} could be attributed to the S=O stretching modes of SO_3 and S_2O, respectively, which could be generated from the secondary reactions of the photolytic intermediates Cl and ClSO.

The 266 nm photon energy (107.5 kcal mol^{-1}) was sufficient for the dissociation of Cl_2SO to Cl + ClSO (D_0 = 57.3 kcal mol^{-1}) and Cl_2 + SO (D_0 = 51.3 kcal mol^{-1}), but not sufficient for SO + 2Cl (D_0 = 108.5 kcal mol^{-1}).[15] The 248 nm excitation led to 3.5 % of the photodissociation via SO ($b^1\Sigma^+$) + Cl_2 and 96.5 % via the ClSO + Cl .[15] In cHex, the most probable photolytic intermediates, ClSO and Cl, were surrounded by the solvent molecules; the corresponding cage effect prevented the immediate escape of the photolytic intermediates, providing an environment for the secondary reaction of Cl and ClSO to generate Cl_2 and SO. In addition, small amounts of the energetic SO ($b^1\Sigma^+$) generated from the molecular elimination channel (Eq. 2) could also lead to the following proposed reactions. Previous gaseous studies have shown that the self-reaction of SO leads to the generation of S_2O_2 (or $S{=}SO_2$),[38,39]

$$SO + SO \rightarrow O{=}S{-}S{=}O \text{ or } SSO_2 \qquad (5)$$

Since the liquid cell was irradiated at 266 nm successively, the S_2O_2 or $S{=}SO_2$ could be further photolysed to generate SO_2 + S, as supported by a recent work from Krasnopolsky,[40]

$$O{=}S{-}S{=}O \text{ or } SSO_2 \xrightarrow{h\nu} SO_2 + S \qquad (6)$$

The generated sulfur atom could quickly react with SO to generate S_2O, since this reaction was estimated as an exothermic process using the predicted absolute energies,

$$S + SO \rightarrow S_2O \qquad \Delta H = -289 \text{ kJ mol}^{-1} \qquad (7)$$

At excitation wavelengths greater than 218 nm, the photodissociation of SO_2 is not energetically allowed,[41] although SO_2 can be excited by 266 nm photons ($\sigma = 4 \times 10^{-19}$ cm^2).[42] The light-induced electronically excited SO_2, denoted as SO_2*, can react with another SO_2 to generate SO_3 and SO,[41]

$$SO_2^* + SO_2 \rightarrow SO_3 + SO \qquad (8).$$

These previous reports[15,38,39,40,41,42] further support our observations that the successive irradiation of the Cl_2SO/cHex in a static cell led to the generation of S_2O and SO_3 and suppressed the generation of SO_2.

Upon successive irradiation of the mixture of Cl_2SO/THF/cHex with 266 nm laser (**Figure 3d**), the spectral features revealed the combinations in **Figure 3b** and **Figure 3c**, including the generation of SO_3 at 1381 cm^{-1}, the suppressed generation of SO_2 at 1345 cm^{-1}, the generation of S_2O at 1156 cm^{-1}, the depletion of neat THF at 1075 cm^{-1}, and the generation of SCl_2–THF at *ca.* 1053 cm^{-1}. Interestingly, an extra band at 1138 cm^{-1} (marked with a star) was observed and might be attributed to the formation of the complex of SO and THF, denoted as SO–THF, before the self-reaction of SO. This assumption is supported by the reduced amount of S_2O. In the absence and presence of THF (**Figure 3c** and **Figure 3d**, respectively), the absorbance ratios $-\Delta Cl_2SO : \Delta S_2O$ were 2 : 1 and 2.5: 1, respectively. Since we proposed that the S_2O generation resulted from the self-reaction of SO, the coordinated SO or the prior photolytic intermediate ClSO by THF was not

capable of supporting the proposed mechanism (Eq. 5) and suppressed the amounts of S_2O and cascading product SO_3. The existence of the ClSO−THF complex is discussed in a later section. Moreover, some vibrational features beneath the bands of S_2O and SO−THF at 1150−1080 cm^{-1} might be attributed to the S=O stretching modes of [S,O] containing species, which were minor products from further secondary reactions upon 266 nm irradiation. Hence, we have demonstrated that THF is able to coordinate to the solutes and the reaction intermediates and to further alter the types and populations of the end products.

Time-resolved difference infrared spectra of Cl_2SO upon pulsed 266-nm excitation in different solvent compositions

The time-resolved difference spectra of Cl_2SO/cHex upon 266 nm irradiation (**Figure 4a**) possessed several transient features, including the depletion of Cl_2SO at 1239 cm^{-1} and upward features at 1155, 1173, and 1212 cm^{-1}. According to the previous photolysis studies of Cl_2SO at 248 nm in the gaseous phase,[16,17] the most probable photolytic intermediate is ClSO, which has been characterized at 1162.9 cm^{-1} in gas phase and attributed to the S=O stretching mode.[17] The predicted wavenumber at 1153 cm^{-1} supports the observed transient species at 1155 cm^{-1}; thus, it was assigned to the S=O stretching mode of ClSO. In addition to the major intermediate, two weak transient features at 1173 and 1212 cm^{-1} could be ascribed to $(ClSO)_2$ via the quick self-reaction of ClSO. $(ClSO)_2$ possessed two S=O vibrational modes at 1200 and 1165 cm^{-1}, in accordance with the prediction, coinciding with the observed doublet at 1212 and 1173 cm^{-1}. Meanwhile, this dynamic association reaction was slightly exothermic by 27 kJ mol^{-1}, in accordance with the prediction, further supporting the aforementioned proposed mechanism,

$$ClSO + ClSO \rightarrow (ClSO)_2 \qquad \Delta H = -27 \text{ kJ mol}^{-1} \qquad (9).$$

The gradual recovery of parent Cl_2SO and decay of the transient species resulted from the slow flow of the photolysis zone out of the detection volume.

The time-resolved difference spectra of Cl_2SO/THF/cHex upon 266 nm pulsed irradiation (**Figure 4b**) possessed similar transient features, except for a new band at *ca.* 1054 cm^{-1}, which was close to the predicted wavenumbers of the C−O−C stretching mode of ClSO−THF. Limited by the spectral resolution of 4 cm^{-1}, the S=O stretching modes of ClSO and ClSO−THF could be indistinguishable since their predicted wavenumbers were separated by 3 cm^{-1}. The ratios ΔAbs(1173 cm^{-1}) / ΔAbs(1155 cm^{-1}) of the Cl_2SO/cHex and Cl_2SO/THF/cHex systems were 0.57 and 0.53, respectively. The reduced ratio in Cl_2SO/THF/cHex referred to the extra contribution at 1155 cm^{-1}; i.e., the spectrally-indistinguishable ClSO−THF without the contribution at 1173 cm^{-1}. This observation supports the reduced amount of S_2O upon the successive irradiation of the Cl_2SO/THF/cHex because the ClSO−THF could alter the cascading secondary reactions that led to the generation of S_2O.

CONCLUSIONS

The photolysis of Cl_2SO at 266 nm in cHex was monitored with time-resolved infrared difference spectroscopy. The density functional theory B3LYP with the conductor-like polarizable continuum model assisted in the assignment of the vibrational features. On the basis of the steady-state spectra and stoichiometry, the major oxygen-containing product of the thermal decomposition of Cl_2SO was SO_2, and the presence of THF resulted in the complexes of SCl_2−THF. Successive irradiation at 266 nm resulted in the major product S_2O with minor SO_3 via secondary reactions involving SO, which was generated from the reaction of the photolytic intermediates Cl and ClSO. The addition of THF decreased the amount of S_2O because the corresponding precursor SO was coordinated by THF, thus reducing the reactivity of SO in the cascading processes. In the

time-resolved difference spectra of Cl_2SO/cHex, an intense transient absorption at 1155 cm^{-1} was attributed to the ClSO, with a small amount of the self-reaction product $(ClSO)_2$ at 1212 and 1173 cm^{-1}. The addition of THF led to an extra band at 1054 cm^{-1}, which was ascribed to the C–O–C stretching mode of the ClSO–THF complex, along with the reduction in the transient amount of $(ClSO)_2$. We have therefore confirmed the coordination ability of THF to the reaction intermediates, which could alter the reaction pathways and the types and population of the end products.

ASSOCIATED CONTENT

The predicted geometries of the relevant molecules are provided in the Supporting Information. This material is available free of charge via the Internet at http://pubs.acs.org.

AUTHOR INFORMATION

Corresponding Authors

* To whom correspondence should be addressed. Telephone: +886-3-5715131 ext. 33396. Fax: +886-3-5711082. E-mail: lkchu@mx.nthu.edu.tw.

NOTES

The authors declare no competing financial interests.

ACKNOWLEDGMENT

The Ministry of Science and Technology of Taiwan (MOST 106-2113-M-007-007-) provided support for this research. M.-C. Shih was supported by a scholarship for College Student Participation in Research Projects from the Ministry of Science and Technology of Taiwan (106-2813-C-007-039-M).

TABLE 1. The vibrational wavenumbers of relevant species using the B3LYP density-functional theory method with the basis sets of aug-cc-pVTZ. The predicted IR intensity (km mol^{-1}) is shown in parentheses. The predicted vibrational properties of the molecules which can be explicitly assigned in the observed spectra are highlighted in bold.

	Absolute energy in cHex (hartree)	S=O associated vibration (cm^{-1})			
		Predicted in cHex	Observed in cHex[$]	Observed in gas	Ref.[&]
S=O (Triplet)	-473.43121344	1145.7 (28)			
S=O (Singlet)	-473.38691576	1144.9 (39)			
O=S=O	-548.71318225	**1322.0 (287)**[as], **1154.9 (38)**[s]	1345[as], 1146[s]	1361.8[as], 1151.4[s]	31
S–S=O	-871.68123505	**1156.3 (245)**	1156	1158.1	32
Cl–S=O	-933.68824513	**1153.0 (129)**	1155[#]	1162.9	17
SO_3	-623.92701989	**1356.4 (246)**[as], **1356.1 (245)**[as], 1045.5 (0)[s]	1381	1391.3	33
$Cl_2S=O$	-1393.93554815	**1235.0 (232)**	1239	1251	33
$S–S=O_2$	-946.90305826	1322.7 (195)[as] 1141.4 (280)[s]			
O=S–S=O	-946.88337937	1080.6 (22)[s], 1034.6 (205)[as]			
$(ClSO)_2$	-1867.38686573	**1200.8 (139)**[s], **1165.2 (424)**[as]	1212[s], 1173[as]		
O=S–THF (Triplet)	-705.97509244	**1142.9 (29)**	1138		
O=S–THF (Singlet)	-705.95107665	1078.8 (123)			
SO_2–THF	-781.26468694	1136.5 (67)[s] 1288.6 (286)[as]			
ClSO–THF	-1166.23290820	**1155.9 (130)**	1155[#]		
$Cl_2S=O$–THF	-1626.48355007	1236.3 (218)			
S-S=O_2-THF	-1179.45671531	1132.9 (277)[s] 1321.8 (198)[as]			
		C–O–C associated vibration in cm^{-1}			
THF	-232.54344933	**1076.0 (137)**	1075	1082	
O=S–THF (Triplet)	-705.97509244	1073.1 (130)			
O=S–THF (Singlet)	-705.95107665	1016.4 (71)			
SO_2–THF	-781.26468694	1044.8 (90)			
Cl_2S–THF	-1551.23042003	1064.6 (117)			
ClSO–THF	-1166.23290820	**1069.8 (116)**	1054		
$Cl_2S=O$–THF	-1626.48355007	1060.9 (107)			
S-S=O_2-THF	-1179.45671531	1031.4 (79)			
		Other molecules			
S (Triplet)	-398.13999617				
S (Singlet)	-398.08054124				
Cl_2	-920.43720152				

Cl_2S	-1318.68378960				

s: symmetric stretch; as: asymmetric stretch; #: spectral overlap of ClSO and ClSO–THF; $: observed in this work; &: observed in gas.

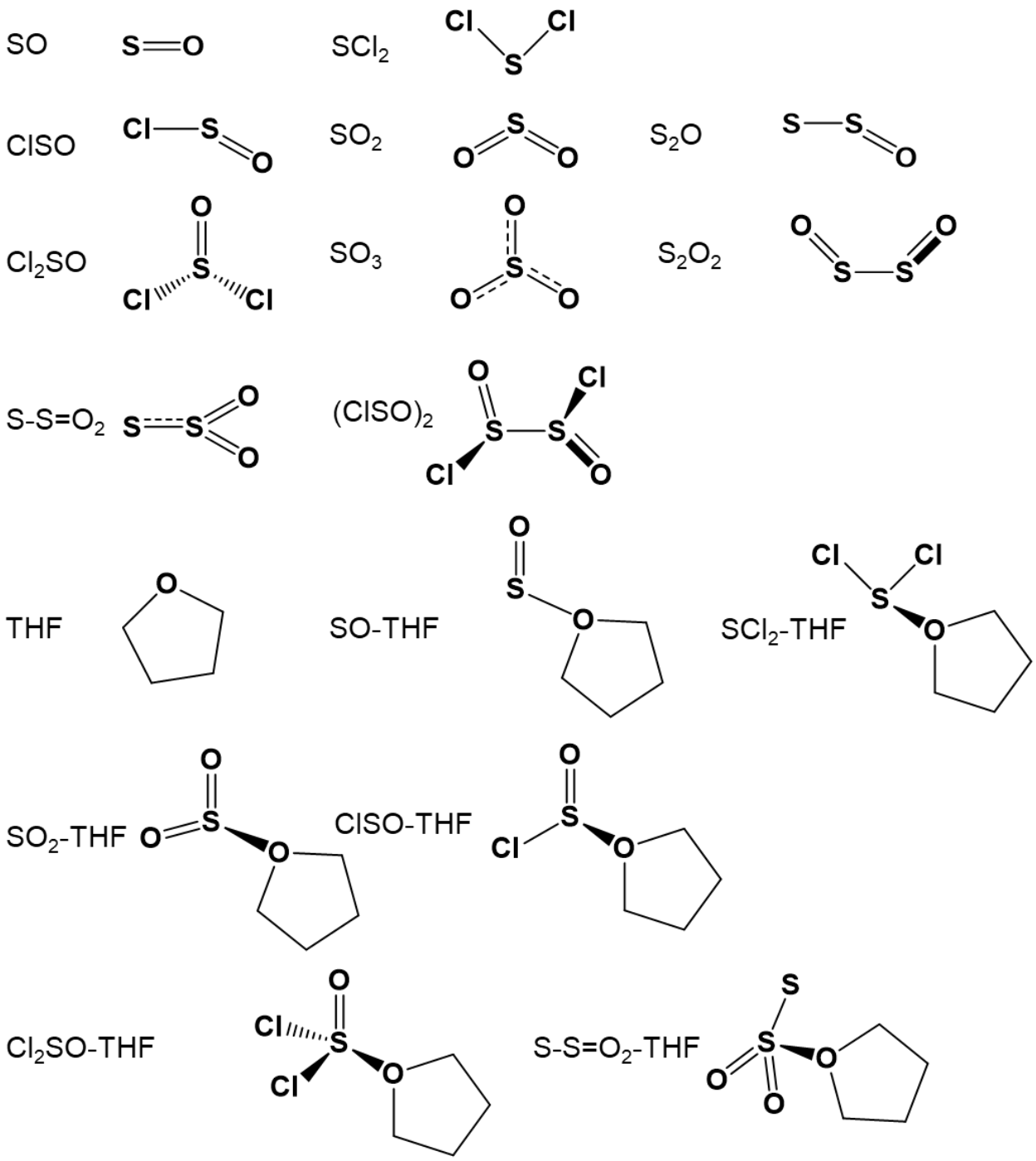

Scheme 1. The formulas of the relevant molecules. The detailed geometries are provided in the Supporting Information.

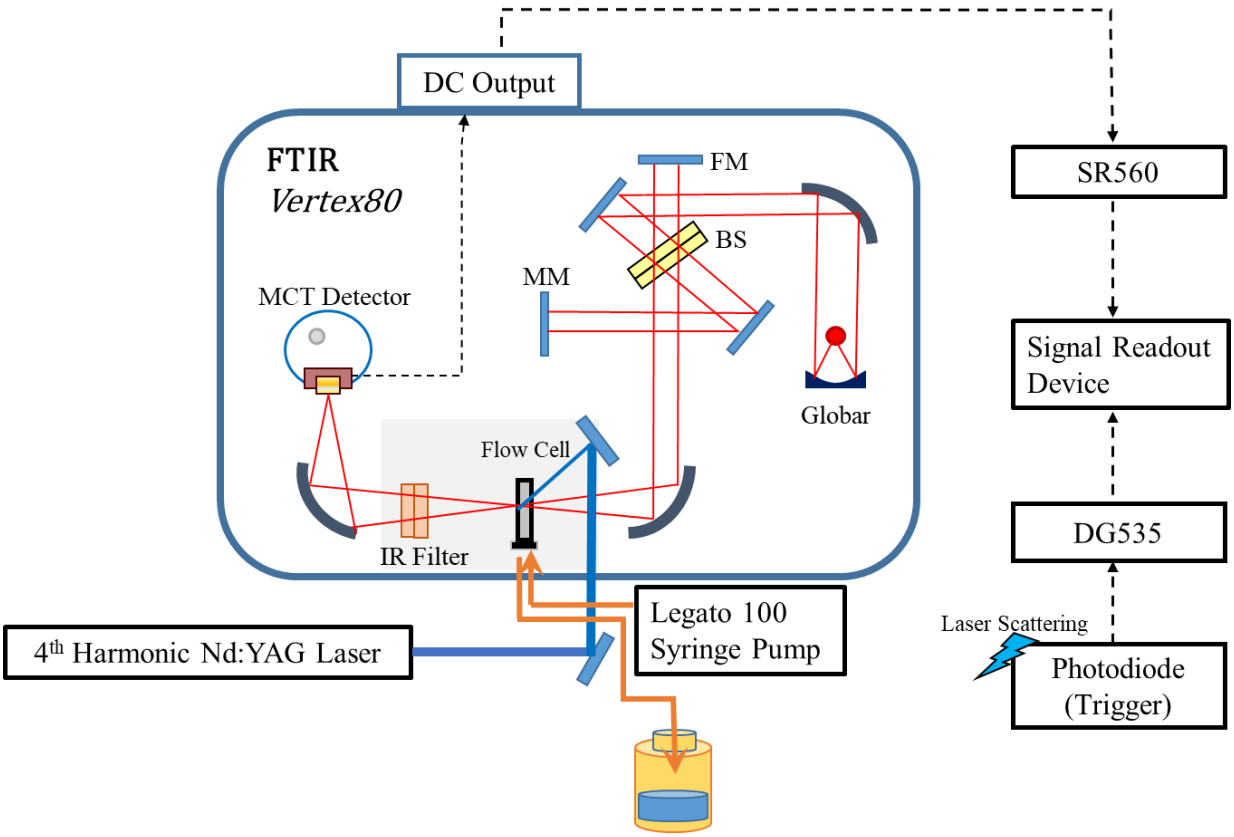

Figure 1. Experimental setup.

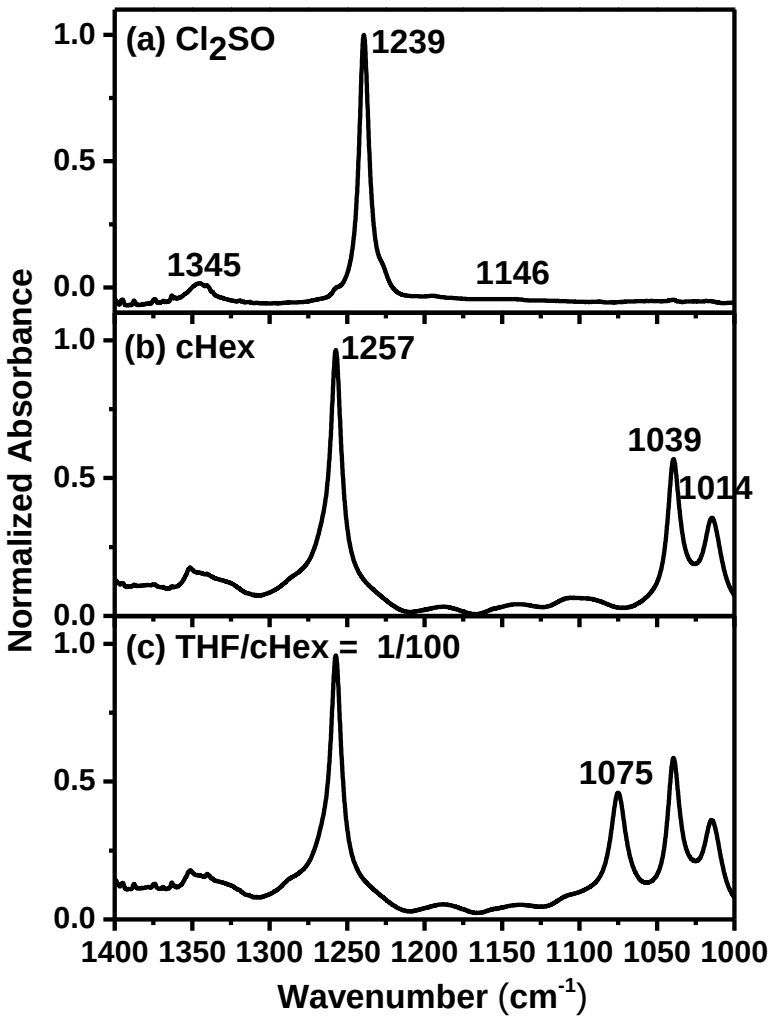

Figure 2. Normalized steady-state infrared absorption spectra of neat (a) Cl_2SO, (b) cHex, and (c) mixture of THF and cHex.

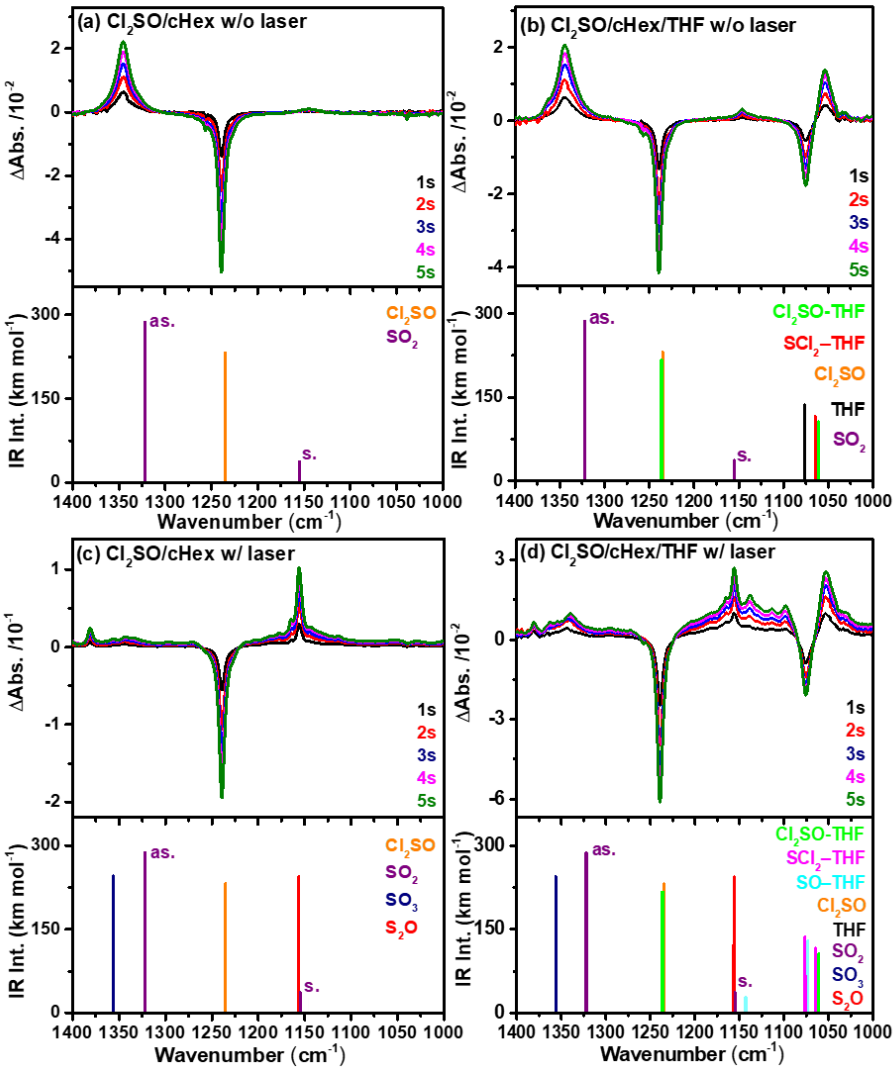

Figure 3. Steady-state IR difference spectra of (a) Cl_2SO/cHex = 1/300 (v/v) and (b) Cl_2SO/THF/cHex = 1/3/300 (v/v/v) without irradiation by 266-nm laser. (c) and (d) denote the aforementioned samples upon successive irradiation with 266-nm laser at 10 Hz with a fluence of 3.14 and 2.67 mJ cm^{-2} for different exposure times. The predicted infrared wavenumbers of the relevant species are shown in stick plots. The heights denote the corresponding infrared absorption intensities.

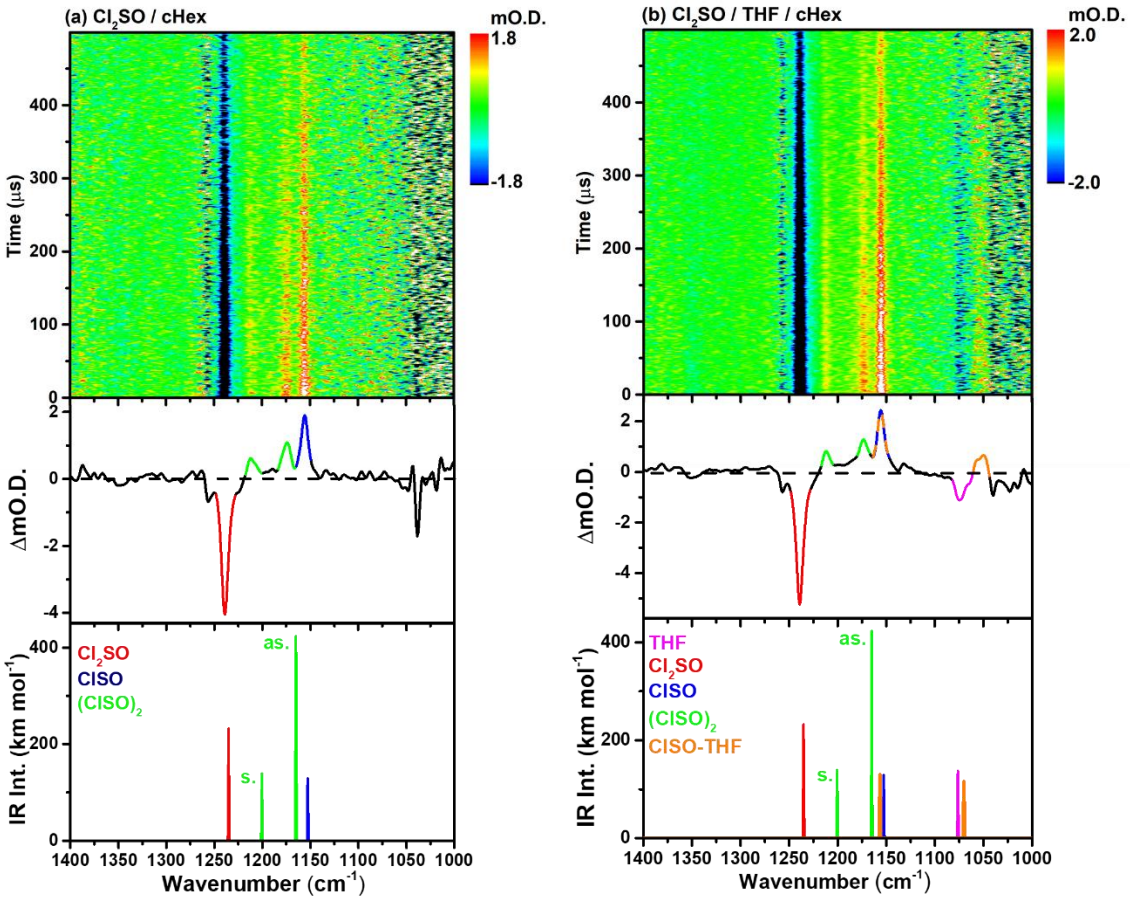

Figure 4. Two-dimensional contours of the time-resolved difference spectra of (a) Cl_2SO/cHex = 1/ 300 (v/v) and (b) Cl_2SO/THF/cHex = 1/2/300 (v/v/v) upon 266 nm irradiation at 10 Hz with a fluence of 5.3 mJ cm^{-2}. The integrated difference spectra in 5–105 μs are compared with the theoretically-predicted vibrational wavenumbers of relevant species shown in stick plots. The heights denote the corresponding infrared absorption intensities.

REFERENCES

(1) Roy, S.; Chatterjee, T.; Islam, Sk. M. Solvent Selective Phenyl Selenylation and Phenyl Tellurylation of Aryl Boronic Acids Catalyzed by Cu(II) Grafted Functionalized Polystyrene. *Tetrahedron Lett.* **2015**, *56*, 779–783.

(2) Ghosh, P.; Das, J.; Sarkar, A.; Ng, S. W.; Tiekink, E. R. T. Oxidation with Selenium Dioxide: the First Report of Solvent-Selective Steroidal Aromatization, Efficient Access to 4β,7α-dihydroxy Steroids, and Syntheses of Natural Diaromatic Ergosterols. *Tetrahedron* **2012**, *68*, 6485–6491.

(3) Malefetse, T. J.; Swiegers, G. F.; Coville, N. J.; Fernandes, M. A. Ion-Pair Structure as a Determinant of Solvent Dependence. Solvent-Selective Formation of *tert*-Butylbis(indenyl)phosphine and *tert*-Butyl(*n*-butyl)indenylphosphine. *Organometallics* **2002**, *21*, 2898–2904.

(4) Rood, J. A.; Landis, A. M.; Forster, D. R.; Goldkamp, T.; Oliver, A. G. Solvent Dependence of the Solid-state Structures of Salicylaldiminate Magnesium Amide Complexes. *Acta Cryst.* **2016**, *C72*, 990–996.

(5) Evans, A. B.; Knight, D. W. Boron Trifluoride–tetrahydrofuran Complex: A Superior Trigger for the Yamaguchi–Hirao Alkylation of Lithio-acetylides by Epoxides. *Tetrahedron Lett.* **2001**, *42*, 6947–6948.

(6) Huang, Y.-H.; Gladysz, J. A. Aldehyde and Ketone Ligands in Organometallic Complexes and Catalysis. *J. Chem. Educ.* **1988**, *65*, 298–303.

(7) Portius, P.; Yang, J.; Sun, X.-Z.; Grills, D. C.; Matousek, P.; Parker, A. W.; Towrie, M.; George, M. W. Unraveling the Photochemistry of $Fe(CO)_5$ in Solution: Observation of $Fe(CO)_3$ and the Conversion between $^3Fe(CO)_4$ and $^1Fe(CO)_4$(Solvent). *J. Am. Chem. Soc.* **2004**, *126*, 10713–10720.

(8) Hermann, H.; Grevels, F.-W.; Henne, A.; Schaffner, K. Flash Photolysis with Infrared Detection. The Photochemistry and Secondary Thermal Reactions of $M(CO)_6$ [M = Cr, Mo, and W]. *J. Phys. Chem.* **1982**, *86*, 5151–5154.

(9) Paur-Afshari, R.; Lin, J.; Schultz, R. H. An Unusual Solvent Isotope Effect in the Reaction of $W(CO)_5$(solv) (solv = Cyclohexane or Cyclohexane-d_{12}) with THF. *Organometallics* **2000**, *19*, 1682–1691.

(10) Grills, D. C.; Huang, K.-W.; Muckerman, J. T.; Fujita, E. Kinetic Studies of the Photoinduced Formation of Transition Metal–dinitrogen Complexes Using Time-resolved Infrared and UV–vis Spectroscopy. *Coord. Chem. Rev.* **2006**, *250*, 1681–1695.

(11) Allen, C. F. H.; Byers, J. R., Jr; Humphlett, W. J., Tishler, M.; Connell, R. Oleoyl Chloride. *Org. Synth.* **1957**, *37*, 66.

(12) Kurzer, F. *p*-Toluenesulfinyl Chloride. *Org. Synth.* **1954**, *34*, 93.

(13) Roth, M.; Maul, C.; Gericke, K.-H. Competitive Channels in the Photodissociation of Thionyl Chloride. *Phys. Chem. Chem. Phys.* **2002**, *4*, 2932–2940.

(14) Kawasaki, M.; Kasatani, K.; Sato, H.; Shinohara, H.; Nishi, N.; Ohtoshi, H.; Tanaka, I. Photodissociation of Cl_2SO at 248 and 193 am in a Molecular Beam. *Chem. Phys.* **1984**, *91*, 285–291.

(15) Wang, H.; Chen, X.; Weiner, B. R. Laser Photodissociation Dynamics of Thionyl Chloride: Concerted and Stepwise Cleavage of S-Cl Bonds. *J. Phys. Chem.* **1993**, *97*, 12260–12268.
(16) Baum, G.; Effenhauser, C. S.; Felder, P.; Huber, J. R. Photofragmentation of Thionyl Chloride: Competition between Radical, Molecular, and Three-Body Dissociations. *J. Phys. Chem.* **1992**, *96*, 156–764.
(17) Chu, L.-K.; Lee. Y.-P.; Jiang, E. Y. Detection of ClSO with Time-resolved Fourier-transform Infrared Absorption Spectroscopy. *J. Chem. Phys.* **2004**, *120*, 3170–3184.
(18) Díaz-Torres, R.; Alvarez, S. Coordinating Ability of Anions and Solvents towards Transition Metals and Lanthanides. *Dalton Trans.* **2011**, *40*, 10742–10750.
(19) Zhao, C.; Wang, D.; Phillips, D. L. Theoretical Study of Samarium (II) Carbenoid ($ISmCH_2I$) Promoted Cyclopropanation Reactions with Ethylene and the Effect of THF Solvent on the Reaction Pathways. *J. Am. Chem. Soc.* **2003**, *125*, 15200–15209.
(20) Huang, Y.-H.; Chen, J.-D.; Hsu, K.-H.; Chu, L.-K.; Lee, Y.-P. Transient Infrared Absorption Spectra of Reaction Intermediates Detected with a Step-scan Fourier-transform Infrared Spectrometer. *J. Chin. Chem. Soc.* **2014**, *61*, 47–58.
(21) Su, Y.-T.; Huang, Y.-H.; Witek, H. A.; Lee, Y.-P. Infrared Absorption Spectrum of the Simplest Criegee Intermediate CH_2OO. *Science* **2013**, *340*, 174–176.
(22) Uhmann, W.; Becker, A.; Taran, C.; Siebert, F. Time-Resolved FT-IR Absorption Spectroscopy Using a Step-Scan Interferometer. *Appl. Spectrosc.* **1991**, *45*, 390–397.
(23) Lórenz-Fonfría, V. A.; Resler, T.; Krause, N.; Nack, M.; Gossing, M.; von Mollard, G. F.; Bamann, C.; Bamberg, E.; Schlesinger, R.; Heberle, J. Transient Protonation Changes in Channelrhodopsin-2 and Their Relevance to Channel Gating. *Proc. Natl. Acad. Sci. U. S. A.* **2013**, *110*, E1273–E1281.
(24) Sun, X. Z.; Nikiforov, S. M.; Yang, J.; Colley, C. S.; George, M. W. Nanosecond Time-Resolved Step-Scan FT-IR Spectroscopy in Conventional and Supercritical Fluids Using a Four-Window Infrared Cell. *Appl. Spectros.* **2002**, *56*, 31–39.
(25) Gaussian 09, Revision A.02, Frisch, M. J.; Trucks, G. W.; Schlegel, H. B.; Scuseria, G. E.; Robb, M. A.; Cheeseman, J. R.; Scalmani, G.; Barone, V.; Petersson, G. A.; Nakatsuji, H. et al. Gaussian, Inc., Wallingford CT, **2016**.
(26) Becke, A. D. Density-functional Thermochemistry. III. The Role of Exact Exchange. *J. Chem. Phys.* **1993**, *98*, 5648–5652.
(27) Lee, C.; Yang, W.; Parr, R. G. Development of the Colic-Salvetti Correlation-energy Formula into a Functional of the Electron Density. *Phys. Rev. B* **1988**, *37*, 785–789.
(28) Dunning, Jr., T. H. Gaussian Basis Sets for Use in Correlated Molecular Calculations. I. The Atoms Boron through Neon and Hydrogen. J. *Chem. Phys.* **1989**, *90*, 1007–1023.
(29) Woon, D. E.; Dunning, Jr., T. H. Gaussian Basis Sets for Use in Correlated Molecular Calculations. III. The Atoms Aluminum through Argon. *J. Chem. Phys.* **1993**, *98*, 1358–1371.
(30) Cossi, M.; Rega, N.; Scalmani, G.; Barone, V. Energies, Structures, and Electronic Properties of Molecules in Solution with the C-PCM Solvation Model. *J. Comput. Chem.* **2003**, *24*, 669–681.
(31) Shimanouchi, T., *Tables of Molecular Vibrational Frequencies Consolidated Volume I*, National Bureau of Standards, **1972**, 1–160.
(32) Müller, T.; Vaccaro, P. H.; Pérez-Bernal, F.; Iachello, F. The Vibronically-resolved Emission Spectrum of Disulfur Monoxide (S_2O): An Algebraic Calculation and Quantitative Interpretation of Franck–Condon Transition Intensities. *J. Chem. Phys.* **1999**, *111*, 5038–5055.

(33) Shimanouchi, T. Tables of Molecular Vibrational Frequencies. Consolidated Volume II. *J. Phys. Chem. Ref. Data* **1977**, *6*, 993–1102.
(34) Futami, Y.; Ozaki, Y.; Hamada, Y.; Wojcik, M. J.; Ozaki, Y. Solvent Dependence of Absorption Intensities and Wavenumbers of the Fundamental and First Overtone of NH Stretching Vibration of Pyrrole Studied by Near-Infrared/Infrared Spectroscopy and DFT Calculations. *J. Phys. Chem. A* **2011**, *115*, 1194–1198.
(35) Futami, Y.; Morisawa, Y.; Ozaki, Y.; Hamada, Y.; Wojcik, M. J.; Ozaki, Y. The Dielectric Constant Dependence of Absorption Intensities and Wavenumbers of the Fundamental and Overtone Transitions of Stretching Vibration of the Hydrogen Fluoride Studied by Quantum Chemistry Calculations. *J. Mol. Struct.* **2012**, *1018*, 102–106.
(36) Richards, T. W.; Shipley, J. W. The Dielectric Constants of Typical Aliphatic and Aromatic Hydrocarbons, Cyclohexane, Cyclohexanone, and Cyclohexanol. *J. Am. Chem. Soc.* **1919**, *41*, 2002–2012.
(37) Cadioli, B.; Gallinella, E.; Coulombeau, C.; Jobic, H.; Berthier, G. Geometric Structure and Vibrational Spectrum of Tetrahydrofuran. *J. Phys. Chem.* **1993**, *97*, 7844–7856.
(38) Herron, J. T.; Hljie, R. E. Rate Constants at 298 K for the Reactions SO + SO + M → $(SO)_2$ + M and SO + $(SO)_2$ → SO_2 + S_2O. *Chem. Phys. Lett.* **1980**, *76*, 322–324.
(39) Frandsen, B. N.; Wennberg, P. O.; Kjaergaard, H. G. Identification of OSSO as a Near-UV Absorber in the Venus Atmosphere. *Geophys. Res. Lett.* **2016**, *43*, 11146–11155.
(40) Krasnopolsky, V. A. Disulfur Dioxide and Its Near-UV Absorption in the Photochemical Model of Venus Atmosphere. *Icarus* **2018**, *299*, 294–299.
(41) Okuda, S.; Rao, T. N.; Slater, D. H.; Calvert, J. G. Identification of the Photochemically Active Species in Sulfur Dioxide Photolysis within the First Allowed Absorption Band. *J. Phys. Chem.* **1969**, *73*, 4412–4415.
(42) Wu, C. Y. R.; Yang, B. W.; Chen, F. Z.; Judge, D. L.; Caldwell, J.; Trafton, L. M. Measurements of High-, Room-, and Low-temperature Photoabsorption Cross Sections of SO_2 in the 2080- to 2950-Å Region, with Application to Io. *Icarus* **2000**, *145*, 289–296.

TOC Graphic